Transient growth and triggering in the horizontal Rijke tube

by

Matthew P. Juniper

reprinted from

International journal of spray and combustion dynamics

Volume 3 • Number 3 • 2011

Multi-Science Publishing
ISSN 1756-8277

Transient growth and triggering in the horizontal Rijke tube

Matthew P. Juniper[1,*]

[1]*Engineering Department, University of Cambridge, Trumpington Street, Cambridge, CB4 1JD, U.K.*

[Submission: July 14, 2010; Revised Submission: March 18, 2011; Accepted: June 14, 2011]

ABSTRACT

This theoretical paper examines a non-normal and non-linear model of a horizontal Rijke tube. Linear and non-linear optimal initial states, which maximize acoustic energy growth over a given time from a given energy, are calculated. It is found that non-linearity and non-normality both contribute to transient growth and that, for this model, linear optimal states are only a good predictor of non-linear optimal states for low initial energies. Two types of non-linear optimal initial state are found. The first has strong energy growth during the first period of the fundamental mode but loses energy thereafter. The second has weaker energy growth during the first period but retains high energy for longer. The second type causes triggering to self-sustained oscillations from lower energy than the first and has higher energy in the fundamental mode. This suggests, for instance, that low frequency noise will be more effective at causing triggering than high frequency noise.

1. INTRODUCTION

Combustion instability has been a long-standing problem in rocket engines and gas turbines. It occurs when pressure fluctuations and heat release fluctuations lock into each other such that instances of higher heat release coincide with instances of higher pressure. In commercial gas turbines, there is a drive to increase the ratio of air to fuel because this leads to lower flame temperatures and therefore lower nitrogen oxide (NOx) emissions. This, however, increases gas turbines' susceptibility to combustion instability.

Recently, there has been considerable interest in the transient growth of thermoacoustic oscillations and the role that non-normality plays in this. Ref. [1] showed that the linearized governing equations of a simple thermoacoustic system, the horizontal Rijke tube, are non-normal and that this non-normality leads to linear transient growth even when all eigenvalues are stable. Ref. [2] found similar behaviour in a Burke-Schumann flame in a tube, a more complex system, which has a higher

*Corresponding Author: mpjl001@cam.ac.uk

degree of non-normality and transient growth than the Rijke tube. These authors explain that the non-normality arises from the convection terms, independently of the acoustics, and is therefore a general feature of combusting systems. Ref. [3] considered a generalized linear thermoacoustic system using the $n - \tau$ model, in which the heat release fluctuation is a linear function of the velocity fluctuation after a time delay. They produced maps of the maximum possible transient growth as a function of n, which represents the thermal intensity, and τ, which represents the time delay. All of these studies show that significant linear transient growth can be achieved in a linearly-stable thermoacoustic system and that this is due to the non-normality of the linearized governing equations.

It is particularly interesting to know whether or not transient growth plays a role in the triggering of thermoacoustic systems. Triggering is a mechanism through which a small perturbation leads to high amplitude self-sustained oscillations even when the corresponding unperturbed system has no unstable eigenvalues. A full description of triggering must include non-linearity in the combustion term and is strongest if the heat release fluctuation is a non-linear function of the velocity fluctuation [4]. These conditions are satisfied by the models of Refs. [1] and [2]. In order to be susceptible to triggering, Ref. [4] shows that a thermoacoustic system must either have a subcritical bifurcation or have a supercritical bifurcation followed by a fold bifurcation in the amplitude/heat-release plane. The role that non-linearity plays in triggering, mode switching and hysteresis has been examined by Ref. [5]. These authors develop and validate a technique for predicting these phenomena, based on an experimentally-derived non-linear Flame Describing Function (FDF), which is used in a frequency domain non-linear stability analysis involving the fundamental mode. Their results show that triggering occurs when the amplitude of an initial perturbation infinitesimally exceeds that of an unstable limit cycle.

The study of Ref. [5] demonstrates triggering but does not include non-normality. This leaves open the possibility that non-normal transient growth can reduce the amplitude of initial perturbations that lead to triggering. This has been considered by Ref. [6], who shows that certain initial perturbations first grow transiently towards an unstable limit cycle and, from there, either grow to self-sustained oscillations or decay to zero amplitude. This is directly analogous to bypass transition to turbulence in hydrodynamic systems [7], in which low amplitude perturbations can first grow transiently towards unstable periodic travelling wave solutions and, from there, either grow to full turbulence or decay to the laminar state [8].

In hydrodynamic systems, the non-linear term conserves the perturbation kinetic energy. This means that, if there is transient kinetic energy growth in a non-normal and non-linear hydrodynamic system, it must be due to non-normality. In thermoacoustic systems, the non-linear term does not conserve the perturbation acoustic energy. This means that, if there is transient acoustic energy growth in a non-normal and non-linear thermoacoustic system, it could arise from non-linearity, non-normality or some combination of the two.

This paper examines a model of the horizontal Rijke tube, which has a small degree of non-normality. Optimal initial states are calculated for both the linear and non-linear

governing equations as a function of the optimization time and their initial energy. By comparing the transient growth from these optimal initial states, the contributions of non-linearity and non-normality can be distinguished. The non-linear optimal initial states are then examined more closely in order to determine the characteristics that lead to triggering.

2. THE MODEL AND ITS GOVERNING EQUATIONS

The system examined in this paper is a horizontal tube with an imposed base flow, in which a hot wire is placed some distance, x_f, from one end [1] [6]. The governing equations are expressed in terms of perturbations on top of a base flow. For example, the velocity perturbation is labelled u' and the base velocity is labelled $\bar{u}$. The fluctuating heat release at the wire, q', is modelled with Heckl's [9] modified form of King's law, shown in Fig. 1. This correlation retains the square root dependence of King's law, $q' \propto |\bar{u} + u'|^{0.5} - |\bar{u}|^{0.5}$, but adds an off-set, $q' \propto |\bar{u}/3 + u'|^{0.5} - |\bar{u}/3|^{0.5}$, which was determined by fitting to experimental results at $u' > 0$ [9]. The off-set creates problems at $u' < 0$ because the heat release should be minimal around $u' = -\bar{u}$, which corresponds to zero velocity at the wire. The results in this paper are for Heckl's modified form, however, so that they can be compared directly with those in Refs. [1] and [6]. Heckl's modified form has the same qualitative form as King's law, so these can be expected to be qualitatively the same as those that would be obtained from King's law. The equations for momentum and energy are non-dimensionalized and then discretized with a Galerkin discretization, which also imposes the boundary conditions. The parameters of the system are: the time delay, τ, between velocity at the wire and heat release; the damping coefficients, ζ_j; and the heat release, β. The governing equations reduce to two delay differential equations (DDEs) for each mode, *j:*

$$F_{1G} \equiv \frac{\mathrm{d}}{\mathrm{d}t}\eta_j - j\pi\left(\frac{\dot{\eta}_j}{j\pi}\right) = 0, \tag{1}$$

$$\begin{aligned} F_{2G} \equiv{}& \frac{\mathrm{d}}{\mathrm{d}t}\left(\frac{\dot{\eta}_j}{j\pi}\right) + j\pi\eta_j + \zeta_j\left(\frac{\dot{\eta}_j}{j\pi}\right)\ldots \\ \ldots{}& + 2\beta\left(\left|\frac{1}{3} + u_f(t-\tau)\right|^{\frac{1}{2}} - \left(\frac{1}{3}\right)^{\frac{1}{2}}\right)\sin\left(j\pi x_f\right) = 0, \end{aligned} \tag{2}$$

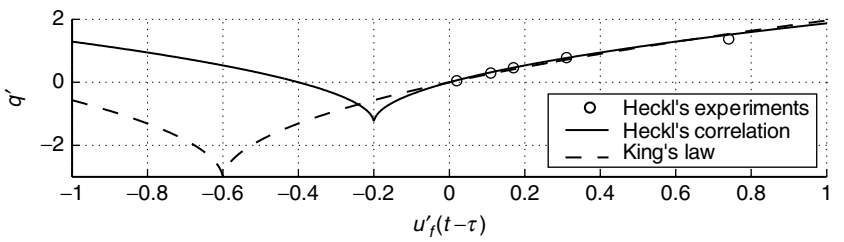

Figure 1: Correlations for the heat release fluctuations q' as a function of the velocity fluctuations u', compared with experimental results for $\bar{u} = 0.6$.

where

$$u_f(t-\tau) = \sum_{k=1}^{N} \eta_k(t-\tau)\cos\left(k\pi x_f\right). \tag{3}$$

The state of the system is described by the amplitudes of the Galerkin modes that represent acoustic velocity, η_j, and those that represent acoustic pressure, $\dot{\eta}_j/j\pi$. These are given the notation $\mathbf{u} \equiv (\eta_1, \ldots, \eta_N)^T$ and $\mathbf{p} \equiv (\dot{\eta}_1/\pi, \ldots, \dot{\eta}_N/N\pi)^T$. The state vector of the discretized system is the column vector $\mathbf{x} \equiv (\mathbf{u}; \mathbf{p})$. 10 Galerkin modes are used in this paper. For the non-linear results, the DDEs eqns (1–2) are integrated with a 4th order Runge-Kutta algorithm from $t = 0$. This requires information about u_f for $t \in [-\tau, 0)$ and, in this paper, u_f is set to zero in this period. For the linear results, the governing equations are linearized in two steps. The first linearization, which is valid for $u_f(t-\tau) \ll 1/3$, is performed on the square root term in eqn (2):

$$\left(\left|\frac{1}{3} + u_f(t-\tau)\right|^{\frac{1}{2}} - \left(\frac{1}{3}\right)^{\frac{1}{2}}\right) \approx \frac{\sqrt{3}}{2}u_f(t-\tau). \tag{4}$$

When eqn (4) is substituted into eqns (1–3), it produces a system of linear DDEs, which in this paper are called the velocity-linearized system. The second linearization, which is valid for the Galerkin modes for which $\tau \ll T_j$, where $T_j \equiv 2/j$ is the period of the j^{th} Galerkin mode, is performed on the time delay:

$$\begin{aligned} u_f(t-\tau) &\approx u_f(t) - \tau\frac{\partial u_f(t)}{\partial t} \\ &= \sum_{k=1}^{N}\eta_k(t)\cos\left(k\pi x_f\right) - \tau\sum_{k=1}^{N}k\pi\left(\frac{\dot{\eta}_k(t)}{k\pi}\right)\cos\left(k\pi x_f\right). \end{aligned} \tag{5}$$

When eqns (4–5) are substituted into eqns (1–3), they produce a system of linear ordinary differential equations (ODEs), which in this paper are called the fully-linearized system.

For the optimization procedure, it is necessary to define some measure of the size of the perturbations. The most convenient measure is the acoustic energy per unit volume, E, because it is easy to calculate and has a simple physical interpretation [3]:

$$E = \frac{1}{2}u^2 + \frac{1}{2}p^2 = \frac{1}{2}\sum_{j=1}^{N}\eta_j^2 + \frac{1}{2}\sum_{j=1}^{N}\left(\frac{\dot{\eta}_j}{j\pi}\right)^2 = \frac{1}{2}\mathbf{x}^H\mathbf{x} = \frac{1}{2}\|\mathbf{x}\|^2, \tag{6}$$

where $\|\cdot\|$ represents the 2-norm. The parameter values used in this paper are $\zeta_j = 0.05j^2 + 0.01j^{1/2}$ and $x_f = 0.3$. Unless specified otherwise, $\tau = 0.02$ and $\beta = 0.75$. The time delay

$\tau = 0.02$ is one quarter of that in the experimental study of Ref. [9]. This time delay would be achieved by using a wire with one quarter of the thickness (i.e. 0.11 mm). These time delays are small compared with those found in typical combusting systems.

For the linear ODEs, the optimal initial states are calculated with the Singular Value Decomposition [7]. The maximum possible transient growth after time T is:

$$G(T) = \max_{\mathbf{x}_0} \frac{\|\mathbf{x}(T)\|^2}{\|\mathbf{x}_0\|^2}. \tag{7}$$

The highest value of $G(T)$, for $T \in [0, \infty]$, is denoted $G_{\max}$ and occurs at time $T_{\max}$. For the linear and non-linear DDEs, the optimal initial states are found with an adjoint looping algorithm embedded within a conjugate gradient optimization algorithm [6].

3. THE BIFURCATION DIAGRAM AND THE 'MOST DANGEROUS' INITIAL STATES

The bifurcation diagram for the system with $\tau = 0.02$ and varying β is shown in Fig. 2. This has been calculated with DDE Biftool [10], which uses a continuation method for DDEs similar to that described by Ref. [11] for ODEs. There is a stable zero amplitude

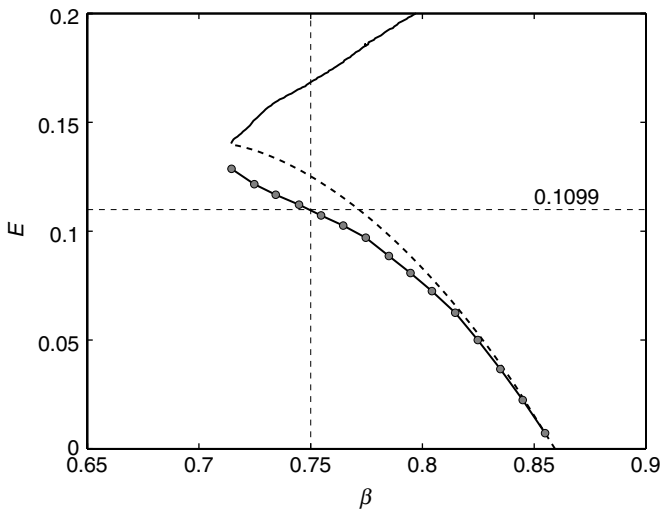

Figure 2: Stable limit cycles (solid line) and unstable limit cycles (dashed line) as a function of the heat release parameter, β. The amplitudes of the limit cycles are quantified by their minimum energy, E. The grey dots show the energy of the lowest energy states that can reach the stable limit cycle [6]. At $\beta = 0.75$, all states with $E_0 < 0.1099$ decay to the zero solution.

solution up to $\beta = 0.859$, at which point there is a subcritical Hopf bifurcation to an unstable limit cycle (dashed line). The unstable limit cycle continues to $\beta = 0.7026$, where there is a fold bifurcation to a stable limit cycle (solid line).

The limit cycles are loops in state space. States on the unstable limit cycle remain on it for all t and are therefore not within the basins of attraction of the zero solution or the stable limit cycle. It is found that some states in the immediate vicinity of the unstable limit cycle are attracted to the zero solution and others to the stable limit cycle. From this it is deduced that the unstable limit cycle lies on the boundary that separates the basin of attraction of the stable limit cycle from that of the zero solution. There are no fixed points on the boundary so, assuming no chaotic dynamics, the unstable limit cycle is the trajectory towards which all points on the boundary converge. It must be stressed that the unstable limit cycle is not the boundary itself (except for the 1 Galerkin mode system [12] §6.2). It merely lies on the boundary. Growth to the stable limit cycle occurs when an initial perturbation starts with infinitesimally higher amplitude than a point on the unstable limit cycle, which is also seen in the results of Ref. [5].

The limit cycles can be represented in several different ways on a bifurcation diagram. For instance, the peak to peak amplitude of the first mode is often plotted on the vertical axis. (For this system, most of the energy is in the first mode when it reaches a limit cycle.) In Fig. 2, the lowest acoustic energy on the limit cycle is plotted on the vertical axis. This representation is chosen because the lowest energy on the unstable limit cycle is the lowest energy on the basin boundary of the stable limit cycle that can be identified with the continuation method. Initial states can grow to the stable limit cycle from lower energy than this but must be found with a different method [6]. Of these states, those with lowest energy have been plotted as circles on Fig. 2. These are known as the 'most dangerous' initial states. The significance for this paper is that initial states with energy below these circles will always decay to the zero solution, even if they grow transiently before then. For $\tau = 0.02$ and $\beta = 0.75$, which are the values chosen in the rest of this study, this initial energy corresponds to $E_0 = 0.1099$.

4. LINEAR OPTIMAL INITIAL STATES

Ref. [1] investigates the optimal initial states of the fully-linearized ODE system while Ref. [6] investigates the most dangerous initial states of the non-linear DDE system. This study starts by investigating the optimal initial state of the velocity-linearized DDE system because this bridges the gap between [1] and [6]. Note that, because the velocity-linearized system is linear, its initial energy is not influential.

Figure 3(top) shows $G(T)$ and $G_{\max}$ for the fully-linearized system (grey line and grey dot) and the velocity-linearized system (dashed line and black dot). For $T < 0.3$, the velocity-linearized system has lower $G(T)$ because, with u_f set to zero during $t \in [-\tau, 0]$, the heat release term in eqn (2) is zero until $T = \tau$ and there is therefore no non-normal transient growth until then. The optimal initial states of the fully-linearized system are similar to those of the velocity-linearized system for the lower Galerkin modes but different for the higher Galerkin modes, for which the

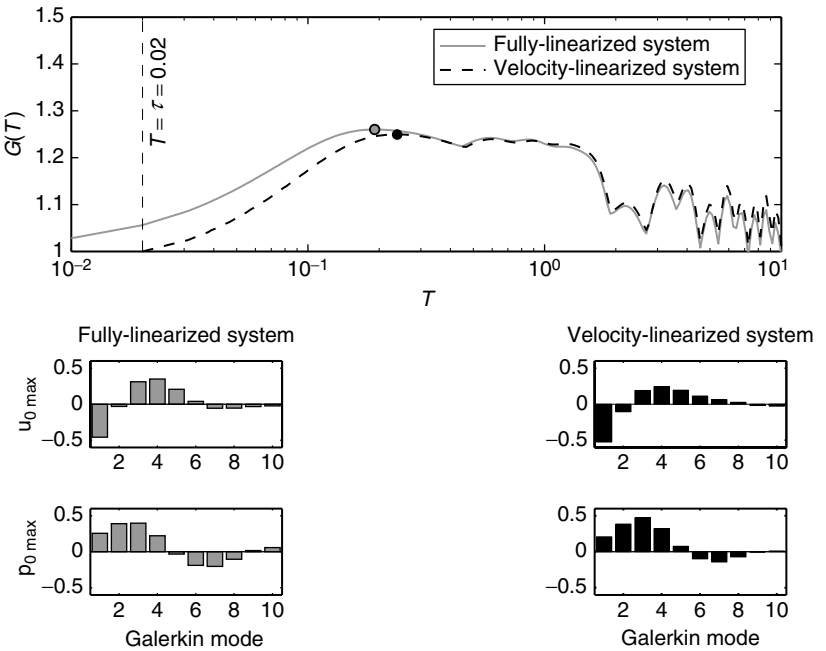

Figure 3: Top frame: $G(T)$ for the fully-linearized system (grey line) and the velocity-linearized system (dashed line) with $\tau = 0.02$ and $\beta = 0.75$. For the fully-linearized system, $G_{max} = 1.2602$ at $T_{max} = 0.1916$ (grey dot). For the velocity-linearized system, $G_{max} = 1.2496$ at $T_{max} = 0.2384$ (black dot). Bottom frames: the optimal initial states for T_{max} of the fully-linearized system (left) and the velocity-linearized system (right).

linearization in time delay eqn (5) becomes increasingly less accurate. For $T > 0.3$, however, the difference between the two is very small.

Although not shown here, the initial states that give rise to $G(T)$ for $T \gg 2$ have most of their energy in the first Galerkin mode because this is the least damped mode.

5. RELEVANCE OF THE LINEAR OPTIMAL INITIAL STATES

When considering transient growth of the non-linear system, it is useful to know whether the linear optimal initial state is relevant. Figure 4 compares the linear (dashed line) and non-linear (solid lines) evolution from the linear optimal initial state for five initial energies: $E_0 = 0.001,0.01,0.1,1$ and 10.

When $E_0 = 0.001$, the non-linear evolution is almost identical to the linear evolution. When $E_0 = 0.01$, the evolution is similar but with slightly higher transient growth. When $E_0 = 0.1$, however, there is very little initial transient growth and when $E_0 = 1$ and 10, there is no initial transient growth at all. It is known from Ref. [6] that an initial energy

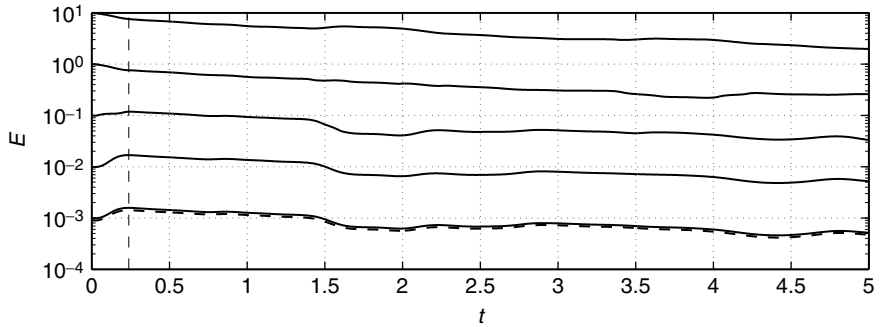

Figure 4: Linear evolution (dashed line) and non-linear evolution (solid lines) from the optimal initial state of the velocity-linearized system with $\tau = 0.02$ and $\beta = 0.75$. The non-linear evolution is shown for $E_0 = 0.001$, 0.01,0.1,1 and 10. $G_{\max}$ of the linear system is achieved at $\tau = 0.2384$ (dashed line).

of at least $E_0 = 0.1099$ is required for this system to trigger to self-sustained oscillations. The linear optimal initial state does not cause significant transient growth at these energies, which suggests that non-linear optimal initial states must be sought in order to investigate whether transient growth influences triggering.

It is important to note that the system being considered here has very small non-normal transient growth. In systems that have larger non-normality, the linear optimal could be more relevant to triggering because the resultant transient growth is considerably larger [2].

6. NONLINEAR OPTIMAL INITIAL STATES

In the linearized systems, G is a function only of T. In the non-linear system, G is also a function of the initial state's amplitude, which in this paper is quantified by the initial acoustic energy, E_0. Therefore $G_{\max}$ is found by optimizing $G(T, E_0)$ over all T and E_0. The algorithm used in this paper finds the optimal initial state for a fine grid of T and E_0 and then extracts $G_{\max}$ from this data.

Refering back to Fig. 3, $G_{\max}$ of the velocity-linearized system is achieved at T = 0.2384 and is equal to 1.2496. Figure 5 plots $G(T = 0.2384)$ as a function of E_0 for the non-linear system. The maximum is achieved at $E_0 = 0.0497$ and is equal to 1.4767. This is significantly higher than $G_{\max}$ of the velocity-linearized and fully-linearized systems. This demonstrates that non-linearity contributes as much as non-normality towards transient growth of this system.

Figure 6 shows contours of G in the (T, E_0)-plane for the non-linear system. Two regions of high transient growth can be seen. The first is centred on $(E_0, T) = (0.050, 0.25)$, with $G_{\max} = 1.48$, and is a continuation of the linear optimal into the non-linear regime. The second is at high values of (T, E_0) and is not a continuation of the linear optimal, which always decays for large T. §7 examines the contribution of these two regions to triggering.

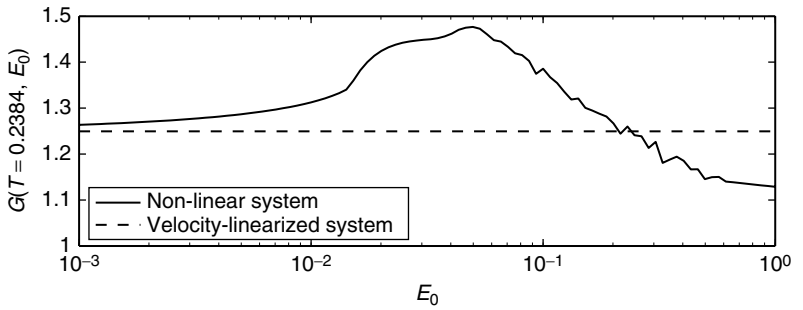

Figure 5: Maximum transient growth, G, at $T = 0.2384$ for the velocity-linearized system and the non-linear system with $\tau = 0.02$ and $\beta = 0.75$. For $E_0 < 0.2$, the non-linear system achieves significantly higher transient growth than the velocity-linearized system.

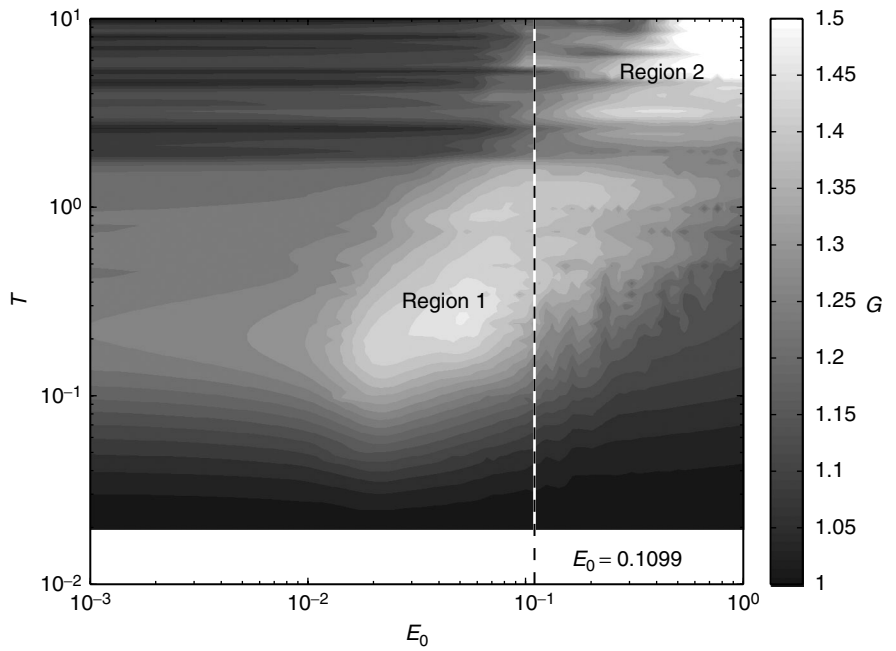

Figure 6: Contours of G in the (T, E_0)-plane for the non-linear system with $\tau = 0.02$ and $\beta = 0.75$. The dashed line shows the triggering threshold, which is the initial energy, E_0, below which all initial states decay to the zero solution [6].

7. RELEVANCE OF THE NON-LINEAR OPTIMAL INITIAL STATES TO TRIGGERING

The dashed line at $E_0 = 0.1099$ in Fig. 6 shows the boundary between the states that cannot trigger to self-sustained oscillations (left) and those that can (right). Firstly, cases that cannot reach self-sustained oscillations are examined. Figure 7 shows $G(T)$ for the velocity-linearized system (dashed line) and $G(T, E_0)$ for the non-linear system at various values of E_0, which are well below that which is required for triggering. In this range of E_0, the maximum transient growth increases as E_0 increases but this effect is confined to the first cycle, $T \in [0, 2]$, which is approximately one period of the fundamental mode. This corresponds to region 1 of Fig. 6.

It is worth commenting on the behaviour of $G(T)$ for $T \in [2, 10]$. G decreases with increasing T because all states decay at long times. G also fluctuates because, once the transient growth during the first period of the fundamental mode has died away, there are two low energy points on each cycle (at 0 and π radians) and two high energy points (at $\pi/2$ and $3\pi/2$ radians). The optimal initial state starts at a low energy point so if the cycle has period $T \approx 2$ and the optimization time is $T \approx 2, 3, \ldots$, the state ends at another low energy point on the cycle and little growth can be achieved. If, however, the optimization time is half way between these, the state ends at a high energy point on the cycle and more growth is achieved.

Figure 8(top) shows G for the non-linear system at $E_0 = 0.1$, which is just below the triggering threshold. There is significant transient growth for $T \in [0, 2]$ and some transient growth at larger T. Figure 8 (middle) shows the amplitudes of the optimal initial states for $T = 0.1, 1.0$ and 10 and Fig. 8 (bottom) shows the evolution from these three optimal initial states. (The evolution of the optimal initial state at $T = T_{max} = 0.398$ is very similar to that for $T = 1$.) The optimal initial state for $T = 10$ produces much less transient growth in the first cycle than that for $T = 0.1$ and $T = 1$. This shows that strong initial transient growth is not a reliable indicator of high amplitudes in the long term.

Secondly, cases that just reach self-sustained oscillations are examined. Figure 9 shows the same information as Fig. 8 but for $E_0 = 0.10999$, which is the triggering threshold. Despite having lower transient growth during the first cycle, the optimal

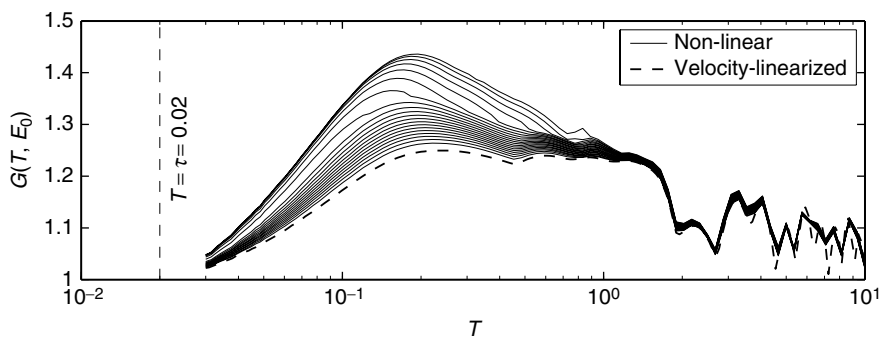

Figure 7: $G(T, E_0)$ as a function of T for the non-linear system with E_0 evenly spaced between 0.001 and 0.020 and with $\tau = 0.02$ and $\beta = 0.75$.

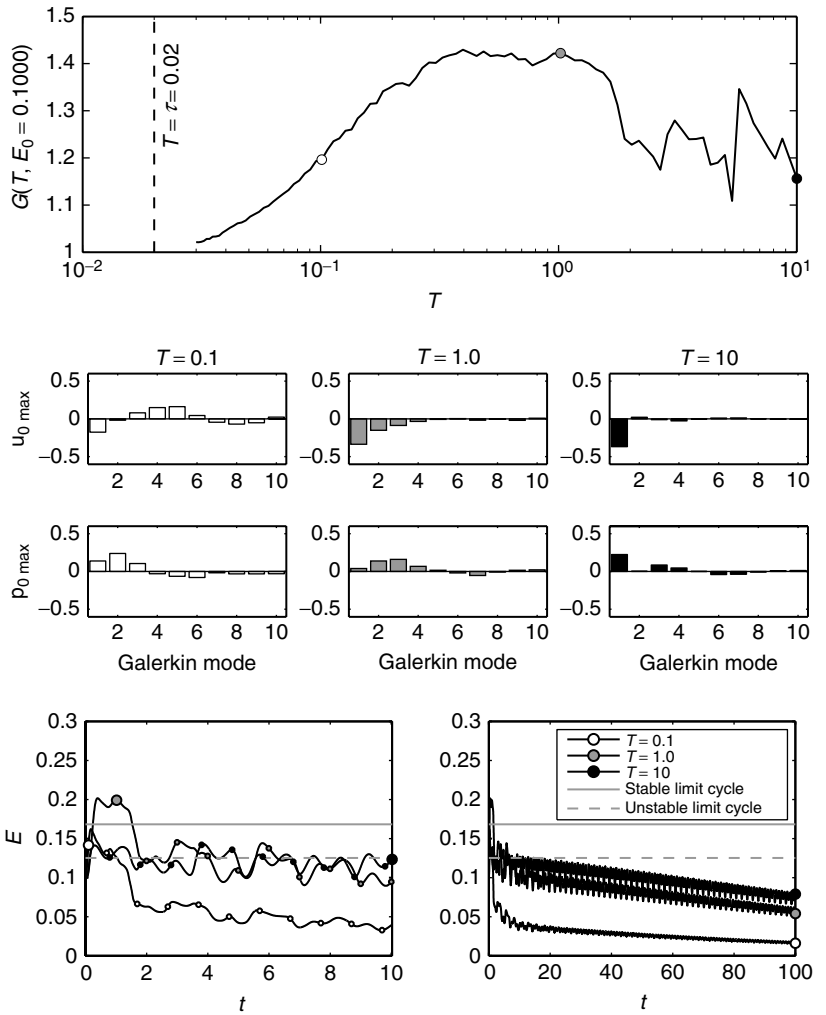

Figure 8: Top frame: $G(T, E_0)$ for the non-linear system with $E_0 = 0.1$, $\tau = 0.02$ and $\beta = 0.75$. Middle frames: the initial states that give maximum G after $T =$ 0.1,1.0 and 10, shown as dots in the top frame. Bottom frames: Evolution in time from these initial states for $t \in [0, 10]$ and $t \in [0, 100]$.

initial state for $T = 10$ is attracted towards the unstable limit cycle, while that for $T = 1$ decays straight to zero. Similarly, Fig. 10 compares the optimal initial state with highest G in Fig. 9 with the most dangerous initial state for this system [6]. The initial state with highest G has high transient growth in the first cycle but then decays straight to zero. On the other hand, the most dangerous initial state has modest transient growth in the first cycle but is subsequently attracted towards the unstable limit cycle and from there

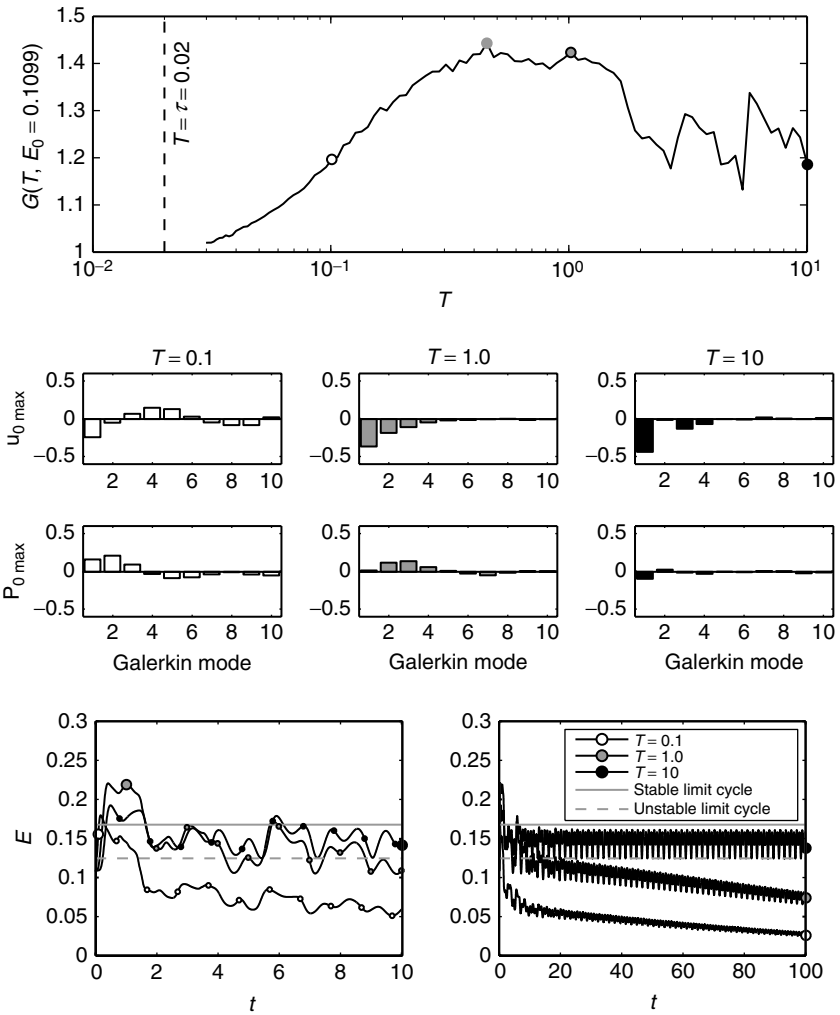

Figure 9: As for Fig. 8 but for $E_0 = 0.1099$, the triggering threshold. The dot at $T = 0.453$ in the top frame shows the initial state with highest G. The line corresponding to $T = 10$ in the bottom right frame continues along the unstable limit cycle indefinitely because it is on the triggering threshold.

grows to the stable limit cycle. The bottom left frame shows the evolution of $\int_0^t E(t')\mathrm{d}t'$ due to the heat release term ($\int_0^t p'q'\mathrm{d}t$) and $\int_0^t E(t')\mathrm{d}t'$ due to the damping term ($\int_0^t \zeta p'^2\mathrm{d}t$). At early times, the former exceeds the latter. At later times, they have the same average gradient, showing that the heat release is balancing the damping. The

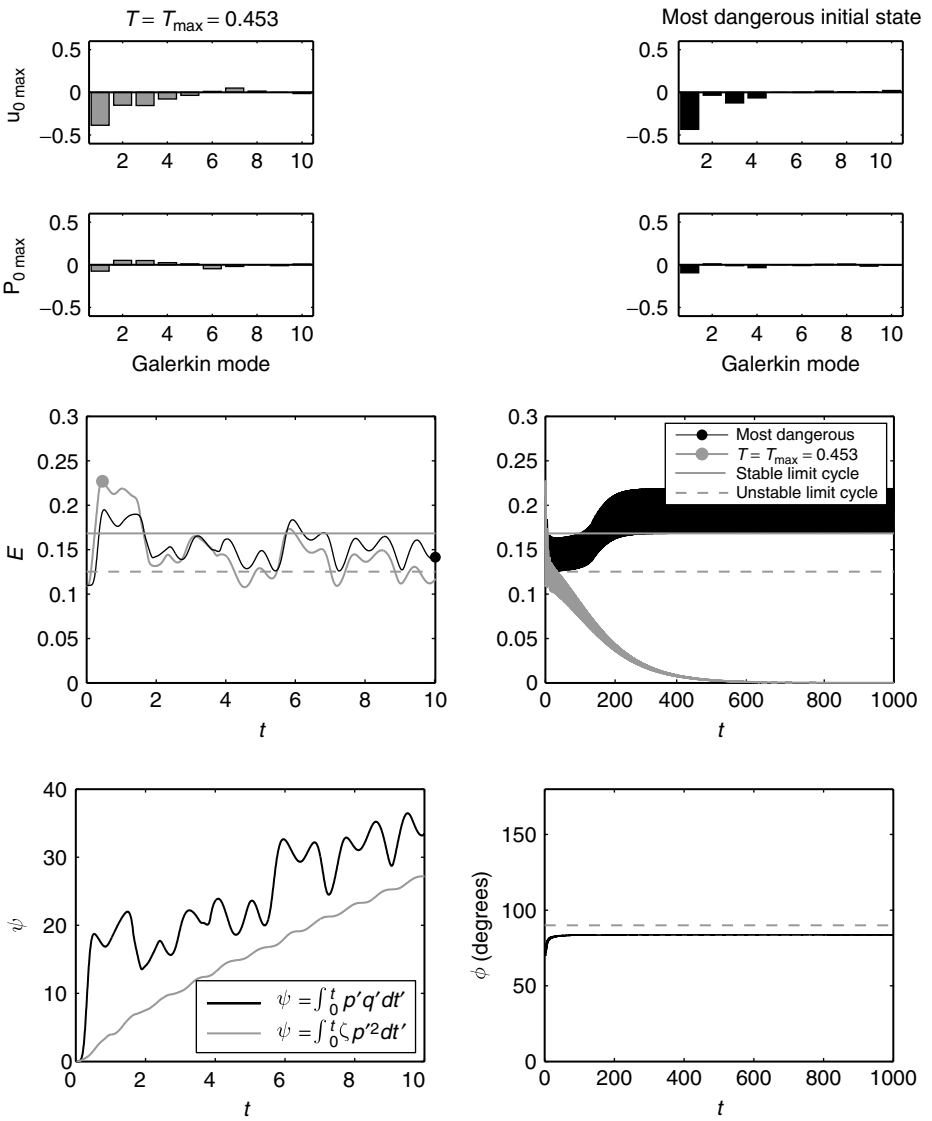

Figure 10: As for Fig. 9 but for the initial state with highest G (top left), which is at $T = 0.453$ in Fig. 9, and for the most dangerous initial state found in Ref. [6] (top right). The bottom left frame shows the evolution of $\int_0^t E(t')\mathrm{d}t'$ due to the heat release term ($\int_0^t p'q'\mathrm{d}t$) and $\int_0^t E(t')\mathrm{d}t'$ due to the damping term ($\int_0^t \zeta p'^2\mathrm{d}t$). The bottom right frame shows the evolution of the phase between p' and q'.

bottom right frame shows the evolution of the phase between p' and q'. The phase adjusts until, at the limit cycle, it is nearly 90° (grey line) and is adding just enough energy per cycle to counteract the damping.

Figure 6 can now be interpreted more clearly. Initial states in region 1 have strong transient growth in the first cycle but decay in later cycles. Initial states in region 2 have weaker transient growth in the first cycle but retain higher energy for longer and are the first to trigger as E_0 is increased past the triggering threshold at $E_0 = 0.1099$. The initial states in region 2 achieve this by maximizing their growth towards the unstable limit cycle, rather than by maximizing their growth overall.

8. CONCLUSIONS

This paper examines transient energy growth and triggering in a model of the horizontal Rijke tube. It provides a clearer link between work on linear transient growth [1] [2] and work on non-linear triggering [4]. A linear analysis shows that the governing equations are non-normal and that this causes transient growth. The linear optimal initial states are calculated and are shown to be relevant to the non-linear system when their amplitudes are small. The non-linear optimal initial states are then calculated, for general amplitudes, and shown to lead to significantly higher transient growth than the linear optimal states. This shows that, in this model, non-linearity contributes to transient growth as much as non-normality does. This differs from hydrodynamics, where the non-linearity conserves energy and therefore does not contribute to transient energy growth.

The maximum transient growth, G, is calculated over a wide range of T and E_0. This reveals two regions of high transient growth (Fig. 6). Region 1 corresponds to initial states that have strong transient growth during the first cycle of the fundamental mode but do not necessarily lead to self-sustained oscillations. Region 2 corresponds to initial states that, near the triggering threshold, maximize their growth towards the unstable limit cycle, rather than maximizing their overall growth. (Far above the triggering threshold, states can grow directly to the stable limit cycle.) The initial states that trigger to self-sustained oscillations from the lowest energy are in region 2. They have most of their energy in the lower Galerkin modes, which suggests that lower frequency noise will be more effective at triggering self-sustained oscillations than high frequency noise.

REFERENCES

[1] K. Balasubramanian and R.I. Sujith. Thermoacoustic instability in a rijke tube: non-normality and nonlinearity. *Phys. Fluids*, 2008, 20:044103.

[2] K. Balasubramanian and R.I. Sujith. Non-normality and nonlinearity in combustion-acoustic interaction in diffusion flames. *J. Fluid Mech.*, 2008, 594:29–57.

[3] S. Nagaraja, K. Kedia, and R. I. Sujith. Characterizing energy growth during combustion instabilities: singularvalues or eigenvalues. *Proc. Comb. Inst*, 2009, 32:2993–2940.

[4] N. Ananthkrishnan, S. Deo, and F. Culick. Reduced-order modeling and dynamics of nonlinear acoustic waves in a combustion chamber. *Combust. Sci. Tech.*, 2005, 177:221–247.

[5] N. Noiray, D. Durox, T. Schuller, and S. M. Candel. A unified framework for nonlinear combustion instability analysis based on the flame describing function. *J. Fluid Mech.*, 2008, 615:139–167.

[6] M.P. Juniper. Triggering in the rijke tube: non-normality, transient growth and bypass transition. *J. Fluid. Mech.*, 2011, 667:272–308.

[7] P. J. Schmid. Nonmodal stability theory. *Annu. Rev. Fluid Mech.*, 2007, 39:129–162.

[8] J. D. Skufca, J. A. Yorke, and B. Eckhardt. Edge of chaos in a parallel shear flow. *Phys. Rev. Lett.*, 2006, 96:174101.

[9] A. Heckl. Nonlinear acoustic effects in the rijke tube. *Acustica*, 1990, 72:63.

[10] K. Engelborghs, T. Luzyanina, and D. Roose. Numerical bifurcation analysis of delay differential equations using dde-biftool. *ACM Trans. Math. Softw.*, 2002, 28:1–21.

[11] C.C. Jahnke and F.E.C. Culick. Application of dynamical systems theory to nonlinear combustion instabilities. *J. Propul. Power*, 1994, 10:508–517.

[12] S. H. Strogatz. *Non-linear dynamics and Chaos.* Perseus, 1991.